Study of Edge Plasma Characteristics at H-mode Transition in Heliotron J

S. WATANABE, K. NAGASAKI[1)], T. MIZUUCHI[1)],S. KOBAYASHI[1)], H. OKADA[1)], K. KONDO, S. YAMAMOTO[2)], Y. TORII[3)], M. KANEKO[4)], H. ARIMOTO, G. MOTOJIMA, Z. FENG[5)], M. NOSAKU, T. TOMOKIYO, S. MATSUOKA and F. SANO[1)]

Graduate School of Energy Science, Kyoto University, Uji 611-0011, Japan
[1)]*Institute of Advanced Energy, Kyoto University, Uji 611-0011, Japan*
[2)]*Graduate School of Engineering, Osaka University, Suita 565-0871, Japan*
[3)]*High Temperature Plasma Center, The University of Tokyo, Kashiwa 277-8568, Japan*
[4)]*National Institute for Fusion Science, Toki 509-5292, Japan*
[5)]*Southwestern Institute of Physics, Chengdu 610041, China*

(Received 5 December 2006 / Accepted 9 April 2007)

Characteristics of spontaneous transition to a high confinement mode (H-mode) have been studied in a helical-axis heliotron device, Heliotron J. The radiation profile measured with a silicon photodiode array shows that a interesting change in the profile occurs at the plasma edge region in the transition phase, forming a strong gradient near the last closed flux surface (LCFS). Relating to the transition, characteristics of bursty density and particle-flux fluctuations current in the scrape off layer (SOL) have been investigated. The probability distribution function for the fluctuations has a tail structure in the L-mode phase, while the tail is suppressed and its direction is reversed after the transition, which may be related to the suppression of edge-plasma turbulence.

Keywords: Heliotron J, H-mode transition, radiation profile, edge plasma turbulence, PDF

DOI: 10.1585/pfr.2.S1059

1. Introduction

Improvement of plasma confinement is one of major issues for realizing attractive fusion reactors. The transition to the edge transport barrier (ETB) formation have been observed in several helical devices such as W7-AS [1], Heliotron J [2], CHS [3] and LHD [4] as well as tokamaks [5–7]. Although the transition phenomena observed in different toroidal devices under various conditions indicate the existence of common plasma physics for the ETB formation, it is not fully understood yet especially in helical systems. The clarification of the transition phenomena observed in helical systems is important to make progress in the understanding the transition physics.

The transition phenomena in Heliotron J were reported in Refs. [8–10]. The increase in stored energy and electron density is observed after the spontaneous drop of the H_α/D_α emission intensity. These observations are similar to the characteristics of the H-mode in tokamaks. The moderate increases in the stored energy and electron density are also observed before the transition. A low frequency fluctuations (dithering) are observed in the H_α/D_α, soft-X ray in some magnetic configuration in this phase [8]. In SOL plasma density and floating potential measured with Langmuir probes, the high-frequency bursting fluctuations are usually observed beside the dithering phenomena. Although the edge plasma fluctuation has been studied experimentally in Heliotron J [11], the fluctuation characteristics in the intermittent bursts during the transition are not fully understood yet in this device.

This paper reports the edge plasma characteristics during the L/H transition in Heliotron J, focusing on the difference of radial profile of radiation measured with a silicon photodiode array among different three field configurations, and statistical characteristics of the edge plasma turbulence at the standard configuration measured with Langmuir probes.

2. Experimental Setup

Heliotron J is a medium size helical-axis heliotron device ($< R_0 > = 1.2$ m, $a = 0.1$-0.2 m, $B_0 < 1.5$ T). The coil system consists of an $l/m = 1/4$ continuous helical coil, two sets of toroidal coils and three pairs of vertical field coil. The combination of these coil sets produces flexible helical-axis heliotron fields. The two sets of toroidal coils can control the bumpiness component of the field in Boozer coordinates, $\varepsilon_b = B(m/n = 0/4)/B(m/n = 0/0)$. The bumpiness is an important component in the helical-axis heliotron configuration because of its contribution to neoclassical transport and improved particle confinement. For plasma initiation and heating, second-harmonic X-mode ECH (70 GHz 0.4 MW) is applied where the mi-

author's e-mail: w.shinya@center.iae.kyoto-u.ac.jp

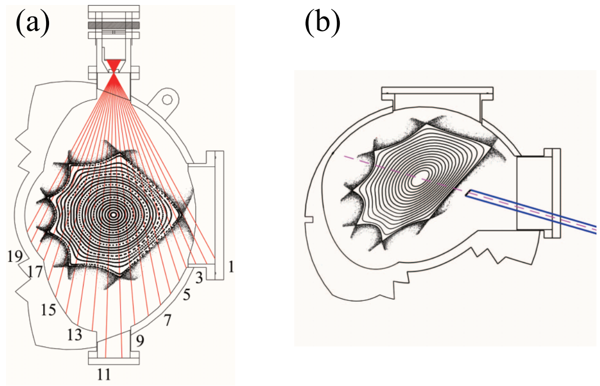

Fig. 1 Poloidal cross-sections showing (a) lines of sight of 20-ch silicon photodiode array and magnetic surfaces for the standard configuration (ε_b = 0.06), (b) position of the movable Langmuir prove.

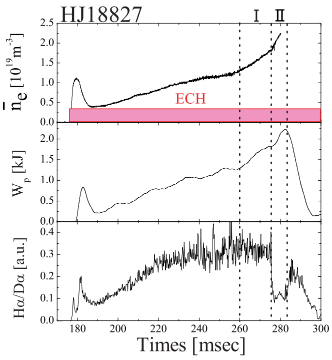

Fig. 2 Time evolutions of density, stored energy and H_α/D_α signals in the standard configuration (ε_b = 0.06).

crowaves are injected from a top port of the torus. The details of the plasma radiation profile. The detector covers the photon energy range from the visible to soft-X ray. Fig. 1 (a) illustrates the lines of sight of the detector array and magnetic flux surfaces for the standard configuration in Heliotron J. The detector covers the edge region of both inside and outside torus. The fluctuation on the edge plasma is measured with a movable Langmuir probe set inserted in scrape off layer (SOL) as shown in Fig. 1 (b). The probe set measures the ion-saturation current and the floating potential simultaneously.

3. Edge Plasma Characteristics During L/H Transition

3.1 Time evolution of radiation profile

Figure 2 shows the time evolutions of electron density n_e, stored energy W_p and H_α/D_α signals for an ECH discharge in the standard configuration (ε_b = 0.06). In the time span of 260-276 ms (phase I), the electron density and the stored energy increase moderately and then the H_α/D_α signal drops down at t = 276 ms (the transition). and the density and stored energy rapidly increase until t = 283 ms. We define this H-mode phase as phase II in this paper. The time evolution of the photodiode signal at edge region is shown in Fig. 3 (a). The signal from edge channels drops down in phase II, while those from core channels increases. Fig. 3 (b) shows time evolution of the relative change rate of the diode signals normalized by the intensity of each channel at 275 ms (t_0) before the start of the phase II, $I(k,t)/I(k,t_0)$, where $I(k,t)$ means the intensity from k-ch of the array at the time of t. These values at outside of the last closed flux surface (LCFS) drop just after the start of Phase II, and then increase asymmetrically near the LCFS. It suggests that the transition causes the change in the radiation profile near the LCFS. The rate of the measured radiation from LCFS is different between the lines of sight in inboard and outboard torus. To focus on the change in the edge radiation profile, the gradient index as follows. First, the difference of the intensities $\Delta I(t)$ between adjacent two channels inside and outside of LCFS. In case of the standard configuration (see Fig. 1 (a)), the indexes are $\Delta I(t) = I(3\text{ch},t)–I(2\text{ch},t)$ on the outboard side and $\Delta I(t) = I(18\text{ch},t)–I(19\text{ch},t)$ on the inboard side. Then $\Delta I(t)$ is normalized by $\Delta I(t_0)$ the value just before the transition. The time evolution of the gradient indexes of the radiation profile for inboard and outboard sides of the torus are shown in Fig. 4 (a). The gradient indexes increase modestly in phase I, and rapidly increase after the start of phase II. This means that a strong gradient in radiation profile is formed near the LCFS. Fig. 5 shows profiles of the radiation in the edge region at each phase, where the intensity is normalized by the signal intensities of ch4 for the outboard side and that of ch17 for the inboard side. The gradient of the profile is moderate in L-mode, but becomes steep just after the transition (t = 277 ms) as a result of the drop of the signal intensity in SOL. The intensity on LCFS grows with time after the transition. The development of the radiation near the LCFS suggests that the transition affects the edge plasma structure near LCFS. No rapid change of radiation profile is observed in the core region.

The same analysis is applied to data from two other field configurations with different bumpiness, $\varepsilon_b = 0.01$ and 0.15. The global confinement in a low bumpy (ε_b = 0.01) configuration is not so good compared to other medium and high bumpy configurations as reported in Ref. 10. In this configuration, the dithering in the edge relating signals are frequently observed in phase I. The time evolutions of the gradient indexes for this configuration are shown in Fig. 4 (b). The change of the radiation profile in phase I is poloidally asymmetric in the low bumpy case. During the dithering period in phase I, the gradient index at the high field side (the inboard-side) increases, whereas it decreases at the low field side. In order to investigate the dithering region, the amplitude of the dithering for each channel is plotted as a function of the channel number in Figure 6. As shown in the figure, the dithering phenomenon is localized near the LCFS. The dithering might

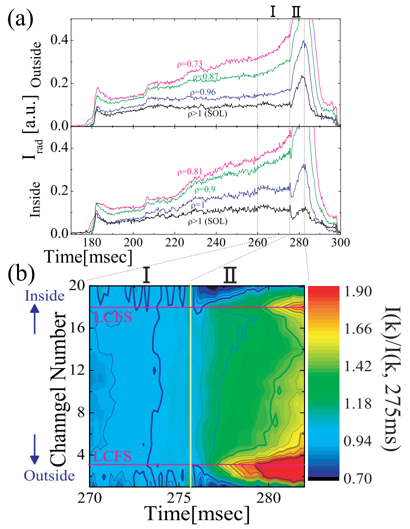

Fig. 3 Time evolution of (a) diode signal (b) normalized relativistic changing rate of diode signal for each channel.

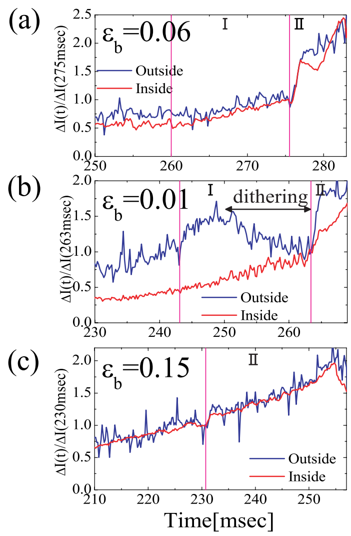

Fig. 4 Gradient index of radiation profile near LCFS, normalized by that just before the transition.

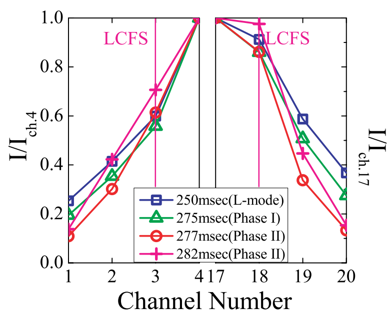

Fig. 5 Change of edge radiation profile at each phase in the standard configuration (ε_b = 0.06).

affect the behavior of the gradient indexes in the phase I near LCFS.

The time evolution of the gradient indexes in the high bumpy configuration is shown Fig. 4 (c). In the high bumpy configuration, the transition is less observed than in the medium and low bumpy cases and the transition occurs without the phase I. Therefore, ΔI is normalized by ΔI at 230 ms before the start of phase II in Fig. 4 (c).The increase of the gradient indexes is observed also in this case, but the increase rate is rather low compared to other two cases and it is almost unchanged during the L-mode phase. The difference suggests that the transition effect depend on the field configuration.

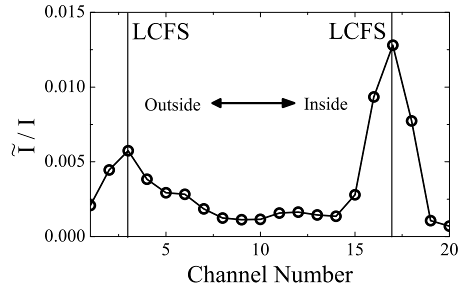

Fig. 6 Fluctuation level for each channel in dithering phase.

3.2 Bursty fluctuation in the edge plasma

As discussed in Sec. 3.1, the change in edge radiation profile is observed in the L/H transition, suggesting that the transition is a phenomenon localized in the plasma edge. In this sub-section, we will discuss the density fluctuation and radial particle flux due to the fluctuation in the standard configuration by using the Langmuir probe data. The density fluctuations and the flux fluctuations are estimated by $\tilde{n} \propto \tilde{I}_{sat}$ and $\tilde{\Gamma} = \tilde{n}\tilde{v} \propto \tilde{I}_{sat}(\tilde{V}_f^1 - \tilde{V}_f^2)$, respectively. Here, I_{sat} is the ion saturation current and $V_f^{1,2}$ are floating potentials with 10 mm distance in the poloidal direction. Fig. 7 shows the time evolution of the ion saturation current and fluctuation-induced flux. Bursting spikes are observed both in the ion saturation current and the flux fluctuation. We have analyzed these signals by using the probability distribution function (PDF). It is well known that the PDF shape should be Gaussian for random turbulence [13]. It was reported [14, 15] that the PDF of the ion saturation current deviates from a Gaussian shape at the SOL region in various magnetic confinement devices. Fig. 8 shows the PDF for the ion saturation current for ECH plasma observed on SOL in Heliotron J. Here, the PDF is normalized by the standard deviation of PDF at each phase. The PDF for the ion saturation current has a positive tail similar as the other magnetic confinement devices. The positive tails of PDF become small in phase I and II and the PDF become nearly Gaussian. The PDF for the fluctuation induced particle flux is shown in Fig. 9. The PDF for the flux also has highly positive tail in the L-mode phase. This positive tail diminishes in phase I, and its direction is reversed in phase II, suggesting the characteristics of the fluctuation induced particle flux is changed at the transi-

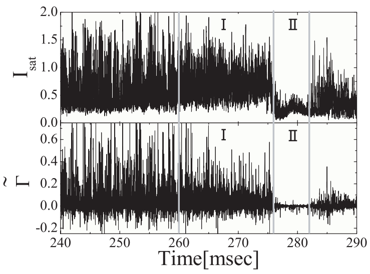

Fig. 7 Time evolution of the ion saturation current and the radial particle flux fluctuation.

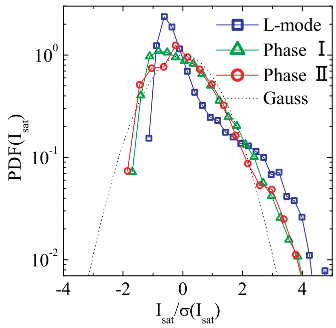

Fig. 8 Probability distribution function (PDF) for ion-saturation current at each phase in medium bumpiness configuration.

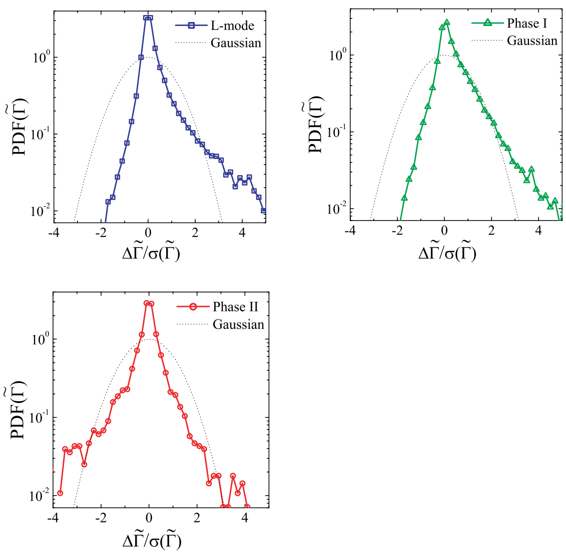

Fig. 9 Probability distribution function (PDF) for radial particle flux fluctuation at each phase in medium bumpiness configuration.

tion. The changes of the bursty characteristics in the ion saturation current might be related to the radial particle flux fluctuation characteristics.

The PDF can be characterized by using the third and forth order moments of fluctuating signal. For a signal denoted by x, the skewness S and kurtosis K are defined as $S = \langle x^3 \rangle / \langle x^2 \rangle^{3/2}$, $K = \langle x^4 \rangle / \langle x^2 \rangle^2$, respectively. The skewness is equal to zero for Gaussian distribution reflecting its symmetry around the average value. The kurtosis can be considered as a measure of the weight of the tails of the distribution, and it is equal to 3 for Gaussian distribution.

Table 1 The skewness and kurtosis for $\tilde{\Gamma}$ at each phase.

$\tilde{\Gamma}$	L-mode	Phase I	Phase II
S	4.2	3.0	-1.2
K-3	23.5	11.8	17.1

Table 1 shows the S and K-3 for the flux fluctuation at each phase. The parameters, S and K-3, are small in the phase I and II, compared to the L-mode. The strong bursts which cause the tail are mitigated in the phase I and II. The kurtosis in phase II is rather large due to the negative tail compared to the phase I. The PDF has negative tail larger than positive tail. The result suggests that the transition suppresses the positive particle transport on the intermittent flux fluctuation.

4. Summary

The radiation profile during the L/H transition in Heliotron J has been investigated by using a 20 channel silicon photodiode array, and bursty characteristics on SOL has been investigated by a Langmuir probe set for the standard configuration.

The change in the radiation profiles during a transition phenomenon suggests that the edge structure is changed near LCFS. The gradient of the edge radiation profile becomes steeper in low and medium bumpiness configurations where the improvement factor is high, while the transition is not so clear in high bumpiness configuration. The difference suggests that the transition effect depend on the magnetic configuration.

The bursty characteristics of the edge plasma turbulence are discussed based on the PDF in standard configuration. The PDF for the fluctuation induced particle flux has a positive tail at the L-mode, but it diminishes and its direction is reversed in the H-mode phase. This change suggests that the outward turbulent transport on busrty flux fluctuation is suppressed. The suppression of the positive tail of PDF distributions has been already observed in phase I. The change in phase I also suggest that the turbulence transport on the busrty flux fluctuation is suppressed in the SOL.

Acknowledgements

The authors are grateful to the other members of the Heliotron J supporting group for their excellent arrangement of the experiments.

[1] V. Erckmann *et al.*, Phys. Rev. Lett. **70**, 2086 (1993).
[2] F. Sano *et al.*, Fusion Sci. Technol. **46**, 288 (2004).
[3] S. Okamura *et al.*, J. Plasma Fusion Res. **79**, 977 (2003).
[4] K. Toi *et al.*, Phys. Plasmas **12**, 020701 (2005).

[5] F. Wagner *et al.*, Phys. Rev. Lett. **53**, 1453 (1984).
[6] J. Lohr *et al.*, Phys. Rev. Lett. **60**, 2630 (1988).
[7] Y. Kamada *et al.*, Nucl. Fusion. **39**, 1845 (1999).
[8] F. Sano *et al.*, Nucl. Fusion. **45**, 1557 (2005).
[9] T. Mizuuchi *et al.*, J. Plasma Fusion Res. **81**, 949 (2005).
[10] T. Mizuuchi *et al.*, Fusion Sci. Technol. **50**, 352 (2006).
[11] T. Mizuuchi *et al.*, J. Nucl. Mater. **337-339**, 332 (2005).
[12] T. Obiki *et al.*, Nucl. Fusion. **41**, 833 (1999).
[13] A.N. Kolmogorov, Dokl. Acad. Nauk SSSR **30**, 301 (1941) (reprinted in Proc. R. Soc. Lond., A 434, 9 (1991)).
[14] Y. Antar *et al.*, Phys. Plasmas **10**, 419 (2003).
[15] van Milligen *et al.*, Phys. Plasmas **12**, 052507 (2005).